THE JOURNAL OF PHYSICAL CHEMISTRY C

Article

Cite This: J. Phys. Chem. C 2018, 122, 15666−15672

pubs.acs.org/JPCC

Selective Polarization Modification of Upconversion Luminescence of $NaYF_4:Yb^{3+},Er^{3+}$ Nanoparticles by Plasmonic Nanoantenna Arrays

Lingxiao Chen,[†] Youying Rong,[†] Mengxin Ren,[‡] Wei Wu,[‡] Mengyao Qin,[†] Chengda Pan,[†] Qiang Ma,[†] Shikang Liu,[†] Botao Wu,*[,†] E. Wu,*[,†,§] Jingjun Xu,[‡] and Heping Zeng[†]

[†]State Key Laboratory of Precision Spectroscopy, East China Normal University, Shanghai 200062, China

[‡]Key Laboratory of Weak-Light Nonlinear Photonics, Ministry of Education, TEDA Institute of Applied Physics and School of Physics, Nankai University, Tianjin 300071, China

[§]Collaborative Innovation Center of Extreme Optics, Shanxi University, Taiyuan, Shanxi 030006, China

Supporting Information

ABSTRACT: Rare-earth ions doped upconversion nanoparticles (UCNPs) have received great attention for the promising applications ranging from bioimaging and sensing to lighting and displaying technology. Meanwhile, active control of polarization state of the upconversion luminescence (UCL) of UCNPs is also significant in the applications such as polarization microscopy and 3D display. Here, we report the polarization modification for the UCL of β-$NaYF_4:Yb^{3+},Er^{3+}$ nanoparticles by selectively matching the localized surface plasmon resonance (LSPR) of the rectangular plasmonic slot nanoantenna array to the spectrum of the UCL. The plasmonic resonance band centered at 650 nm of the nanoantenna array realized a strong polarization nature of the selected UCL around 660 nm with the degree of linear polarization up to ∼80%, which stems from the interaction between the 660 nm emission band of UCNPs and the plasmonic modes of the rectangular slot nanoantenna array. Meanwhile, the UCL at 550 nm remained unpolarized due to the mismatch to the plasmonic modes. The experimental results are explained well by theoretical simulations based on the local surface plasmonic resonance. Our results provide an effective way to control the anisotropic UCL of UCNPs with the applications in polarization-based imaging and 3D display technologies and so forth.

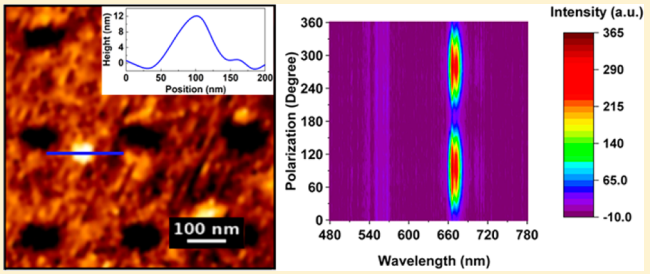

INTRODUCTION

Rare-earth ion doped upconversion nanoparticles (UCNPs) have attracted considerable attention because of their applications in biodetection and imaging,[1−4] photodynamic therapy,[5,6] display technology,[7] and solar cells[8,9] owing to their narrow and tunable emission, high thermal/photostability, large anti-Stokes shifts, and long fluorescence lifetime.[10,11] In the meantime, polarization state modification of upconversion luminescence (UCL) of UCNPs shows great importance in the applications in microscopic multi-information transportation,[12] polarization-based 3D display technologies, and high-resolution imaging.[13] The polarized UCL of rare-earth ions doped single β-$NaYF_4$ nanorods[12] and nanodisk[13,14] as well as $KMnF_3$ nanowire arrays[15] has been reported. By utilizing the intrinsic and strict crystal-field anisotropy of the nanocrystals with the sizes of several hundred nanometers, the UCL exhibits a strong polarization dependence on both the excitation and the emission spectrum. However, when the size of UCNPs is decreased to a few tens of nanometers even several nanometers, it is difficult to modify the UCL polarization state by that because the periodic boundary conditions of nanocrystals are broken due to the size effect of nanomaterials, which results in the crystal lattice distortion of UCNPs.[16] As an alternative, plasmonic metallic nanostructures may be a good approach to modify the UCL of such kind of UCNPs. Surface plasmon resonance, the collective oscillation of conduction electrons on metallic nanostructure surfaces when interacting with incident light, can produce strong near field enhancement localized around the metallic nanostructures, which has been used to greatly promote photochemical reactions[17,18] and amplify the luminescence from nearby optical emitters.[19,20] In particular, this strong near field enhancement for anisotropic metallic nanostructures is very sensitive to light polarization, and has been utilized to modify the fluorescence polarization state of optical emitters. For example, active control of the emission polarization state of fluorescent molecules, single color centers in solids and quantum dots by gold nanorods,[21−24] silver nanoparticles and nanowires,[25,26] nanoparticle dimer,[27−29] bowtie nanoaperture,[30] and anisotropic metallic arrays[31−33] has been achieved. Recently, efforts have also been devoted to modify the UCL polarization state of UCNPs using gold nanorods by carefully attaching UCNPs to gold nanorods.[34,35]

Received: April 27, 2018
Revised: June 15, 2018
Published: June 19, 2018

DOI: 10.1021/acs.jpcc.8b03975
J. Phys. Chem. C 2018, 122, 15666−15672

Rare-earth ion doped UCNPs generally exhibit sharp and multiple-peak UCL. If the polarization state of the individual UCL peaks can be tuned independently, numerous applications of UCNPs including dynamic color tuning,[36] super-resolution polarization imaging,[37] faster fluorescence-based polarization sensors,[38] light-emitting devices,[39] and so forth will be opened up.

Here, we report the selective modifications to the polarization states of UCL at different spectral peaks by coupling the UCNPs with the rectangular plasmonic slot nanoantenna array. Compared with the above anisotropic metal nanostructures, the periodic slot nanoantenna arrays have some advantages, such as reproducible fabrication, planar geometry beneficial to device scaling and miniaturization, systematically tunable plasmonic resonance by designing the slot size. Spherical β-$NaYF_4$:Yb^{3+},Er^{3+} nanoparticles, which pristinely show nonpolarized UCL, were directly deposited on the nanoantenna array. By selectively coinciding the plasmonic resonance of nanoantenna array with the red emission band of UCNPs, we selectively achieved linearly polarized UCL emission around 660 nm. To analyze the polarization state of the emission, the parameter called degree of linear polarization (DOLP) was measured up to 80% around 660 nm. On the other hand, at 550 nm emission band, only about DOLP of 20% was observed due to its large wavelength mismatch, hence negligible interaction with the nanoantenna resonances. This surface plasmon induced polarization state modification to the UCL from UCNPs would play a vital role in applications of polarization-based photodetection and imaging.

EXPERIMENTAL SECTION

The rectangular plasmonic slot nanoantenna array was prepared by focused ion beam milling through the 50 nm thick gold film on a glass substrate.[32] The rectangular slots were patterned in a square unit cell with a pitch of 300 nm and the entire array area is 30 μm × 30 μm. The length and width of the slot was designed to be 80 and 25 nm, respectively. Spherical β-$NaYF_4$:Yb^{3+},Er^{3+} UCNPs were purchased from Changchun Micro Era Technology Co. Ltd., China.

The scanning electron micrograph (SEM) of the plasmonic rectangular slot nanoantenna array was taken by a FEI Helio 600i microscopy operating at 10 kV. The transmission electron microscopy (TEM) images were taken by a JEM-2100F microscopy operating at 120 kV. Power X-ray diffraction (XRD) analysis of the UCNPs was conducted by a diffractometer (Bruker D8 ADVANCE, LynxEye detector, operating at 40 kV and 40 mA) at a scanning step of 0.02° in the 2θ range of 10° to 80° (Cu Kα radiation, λ = 1.5418 Å). The upconversion properties of UCNPs were investigated by a scanning confocal microscope.[11,15,35] UCNPs spin-coated on the substrate was placed on the x−y piezo. The excitation source was a continuous-wave laser at 980 nm. Yb^{3+} ions are sensitizers in β-NaYF4:Yb^{3+},Er^{3+} UCNPs. The maximum absorption of Yb^{3+} ions is at about 975 nm, and thus the commercial 980 nm laser is suitable for the excitation of UCNPs. The laser source was linearly polarized. The followed half-wave plate was used to adjust the polarization direction. The laser beam was reflected by a dichroic mirror and focused on UCNPs by a microscope objective (×100, N.A. = 0.9, MPlanFLN, Olympus) with a focal spot size of ∼1.3 μm. The UCL was collected by the same microscope objective and was spatially filtered by a pinhole with the diameter of 100 μm in a telescope system. With a short-pass filter cutting off at 775 nm, the UCL was detected by the spectrometer (SpectraPro-300i, Acton Research Corporation) and the avalanche photodiode (APD) single-photon detector. And the half-wave plate together with the Glan-Taylor prism before the spectrometer and the APD was employed to verify the polarization state of the UCL.

The numerical simulations were performed by a commercial software based on the finite-difference time-domain (FDTD) method (FDTD Solutions, Lumerical Solution, Inc. Canada). The simulation domain includes one unit cell of the slot nanoantenna array with periodic boundary conditions in both x and y directions and perfectly matched layers in the z direction. The dimension and pitch of the slot in a 50 nm thick film of gold on a quartz substrate was 81 nm ×28 and 300 nm, respectively. A plane wave source ranging from 400 to 1100 nm was illuminated into the simulation domain. The Au dielectric constant was taken from the reference 40 and the refractive index of the surrounding medium was set to be 1.0. A three-dimensional nonuniform meshing was used, and a grid size of 0.5 nm was chosen around the slot. The transmittance and reflectance spectra from the slot nanoantenna array were calculated by using a set of power monitors placed on the upper and lower domain of the nanoantenna array. The electric field enhancement maps at 550, 660, and 980 nm were evaluated using the frequency domain field profile monitors.

RESULTS AND DISCUSSION

SEM image of the rectangular plasmonic slot nanoantenna array is shown in Figure 1a. The Figure 1b depicts the extinction

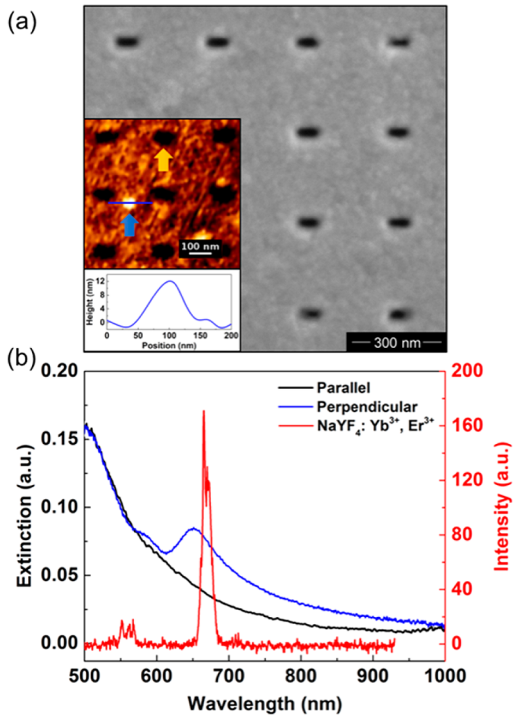

Figure 1. (a) SEM image of rectangular slot nanoantenna array. Inset: AFM topographic image of $NaYF_4$, Yb^{3+}, and Er^{3+} nanoparticles on the nanoantenna array and the line scan. The blue and yellow arrows indicate the single UCNP and the rectangular slot, respectively. (b) Measured extinction spectrum of the nanoantenna array under the plane-wave illumination with the polarization parallel and perpendicular to the long axis of the slots and the UCL spectrum of $NaYF_4$, Yb^{3+}, and Er^{3+} nanoparticles on glass coverslip.

DOI: 10.1021/acs.jpcc.8b03975
J. Phys. Chem. C 2018, 122, 15666−15672

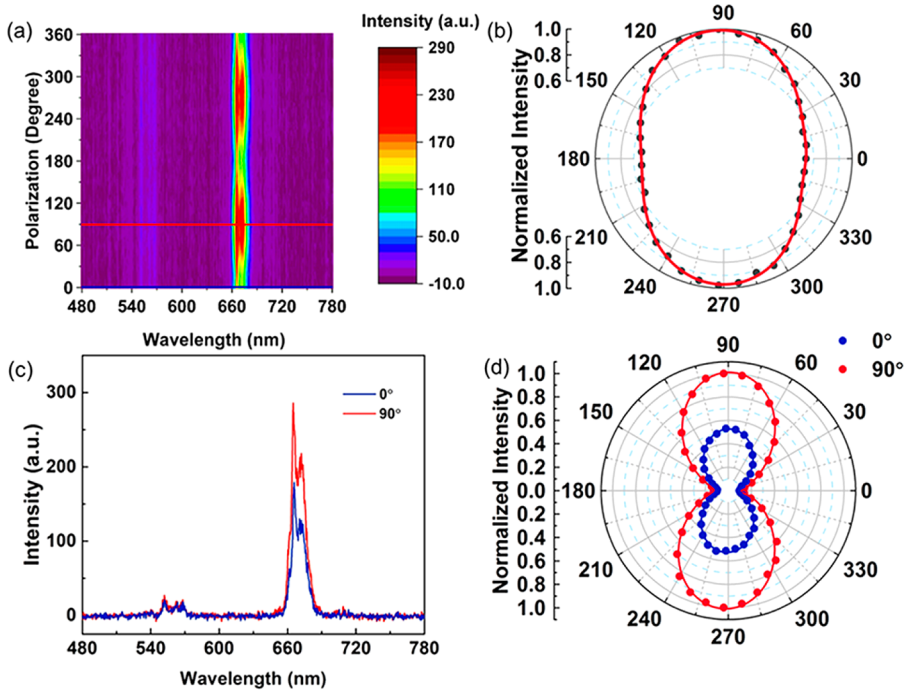

Figure 2. (a) UCL spectra of UCNPs on nanoantenna array as the excitation laser polarization changes. (b) Polar plots of the normalized UCL intensity of UCNPs on nanoantenna array as a function of excitation polarization angle, where the red line is fit for the experimental data. (c) UCL spectra at the excitation polarization of 0° and 90°, respectively. (d) Polar plot of the UCL intensity at different polarization directions under the excitation laser polarization angle at 0° and 90° with fittings.

spectra for the incident light polarization parallel and perpendicular to the long axis of the slots. The spectra demonstrate that a plasmonic resonance of nanoantenna array occurs around 650 nm for the incident light polarization along the short axis of the slots, while almost disappears when the light polarization is along the long axis of the slots. The upconversion nanoparticles were $NaYF_4$:Yb^{3+},Er^{3+} nanocrystals in hexagonal-phase, which was characterized by XRD and TEM (Figure S1 in the Supporting Information), respectively. UCNPs were spin-coated on the nanoantenna array, where UCNPs were distributed with an average number density of 1−2 μm^{-2} (see Figure S2 in the Supporting Information). Under 980 nm excitation, the UCL spectrum of UCNPs shows a weak emission peak at 550 nm and a strong emission peak at 660 nm, which are attributed to the $^2H_{11/2}$, $^4S_{3/2} \rightarrow {}^4I_{15/2}$ and the $^4F_{9/2} \rightarrow {}^4I_{15/2}$ transitions of the Er^{3+} ion, respectively. The UCL peak at 660 nm overlaps the plasmonic resonance of the nanoantenna array as shown in Figure 1b. According to the atomic force microscope (AFM) topographic image as the inset of Figure 1a, the sizes of the UCNPs are about ∼11 nm.

With a laser scanning confocal microscope (as shown in Figure S3), we investigated the excitation polarization sensitivity of UCL of the single $NaYF_4$:Er^{3+},Yb^{3+} nanoparticle on the nanoantenna array. A continuous-wave laser diode at 980 nm with a single-mode fiber pigtail was used to excite the UCL. The laser intensity was maintained at about 400 kW/cm^2 at the focus of the microscope objective during the whole measurements. A half-wave plate together with a Glan−Taylor prism was used to tune the laser polarization orientation. An isolated single $NaYF_4$:Er^{3+},Yb^{3+} nanoparticle on the nanoantenna array could be identified by scanning the sample on the piezo-driven *XYZ* nanopositioning stage. The confocal UCL image of the individual $NaYF_4$:Er^{3+},Yb^{3+} nanoparticle on the nanoantenna array is shown in Figure S4. The polarization direction was defined as 0° for the incident light polarized along the long axis of the nanoantenna slot. As shown in Figure 2a, the UCL spectra vary as the excitation polarization angle changed. The maximal overall UCL intensity from 480 to 780 nm was observed when the excitation polarization was along 90°. And the minimal UCL intensity was obtained when the excitation laser polarized along 0° as shown in Figure 2b. The excitation polarization sensitivity of the overall spectrum was calculated to be ∼21% according to

$$P = \frac{I_\perp - I_\parallel}{I_\perp + I_\parallel} \quad (1)$$

where $I_\perp$ ($I_\parallel$) represents the UCL intensities when the excitation laser polarization angle was at 90° (0°). As the UCL exhibited mainly two peaks in the spectrum, we studied the excitation polarization sensitivity of each peak according to the UCL spectrum under different excitation laser polarization direction. The UCL peak at 660 nm shows a stronger polarization sensitivity on the excitation laser than that at 550 nm as shown in Figure 2c. The excitation polarization sensitivity for the UCL peak at 660 nm was 31% and that of the peak at 550 nm was 17%. Therefore, it can be concluded that the UCL has little polarization sensitivity to the excitation laser, whether the whole spectrum or the individual UCL peak (550 or 660 nm). From the extinction spectra in Figure 1b it can be seen that the slot nanoantenna array has a sensitively polarized plasmonic resonance at 660 nm, while has no obvious plasmonic response at 550 nm. When illuminated by the polarized 980 nm laser, the slot nanoantenna array produces an off-resonance polarized modification on the UCL of UCNP at 660 nm, while it does not happen for that at 550 nm. Therefore, the excitation polarization sensitivity at 660 nm is stronger than that at 550 nm. According to Figure 1b, the nanoantenna array shows a very weak plasmonic response at 980 nm. Therefore, the coupling between

DOI: 10.1021/acs.jpcc.8b03975
J. Phys. Chem. C 2018, 122, 15666−15672

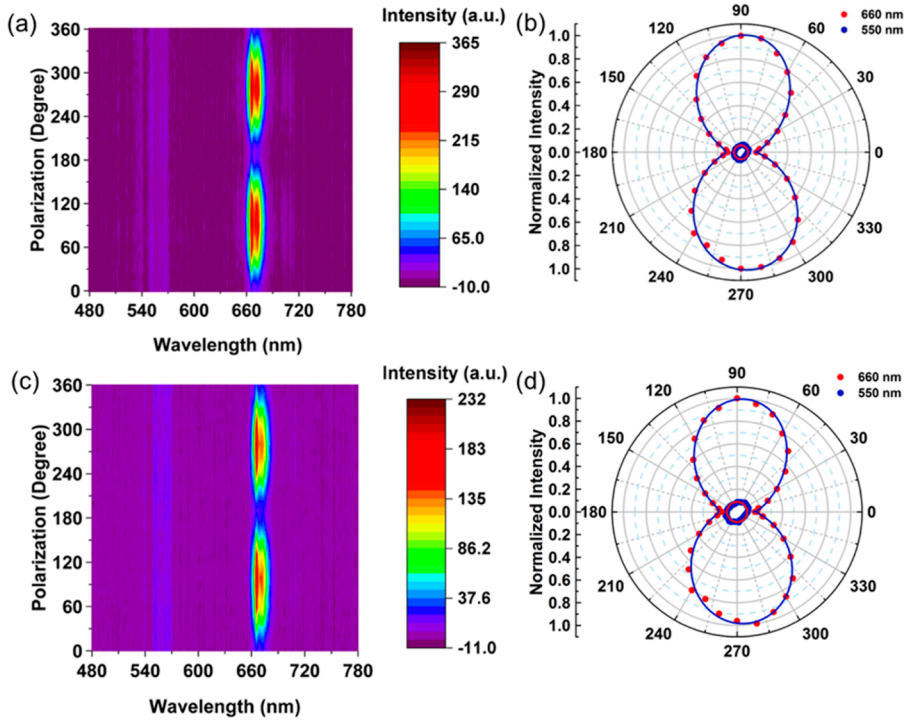

Figure 3. (a) Polarized UCL spectra of UCNPs on plasmonic nanoantenna array under excitation polarization angle at 90°. (b) Polar plot of the normalized UCL intensity at 660 and 550 nm at different emission polarization directions under excitation polarization angle at 90°. (c) Polarized UCL spectra of UCNPs on plasmonic nanoantenna array under excitation polarization angle at 0°. d) Polar plot of the normalized UCL intensity at 660 and 550 nm at different emission polarization directions under excitation polarization angle at 0°. The solid lines are fitting for the experimental data.

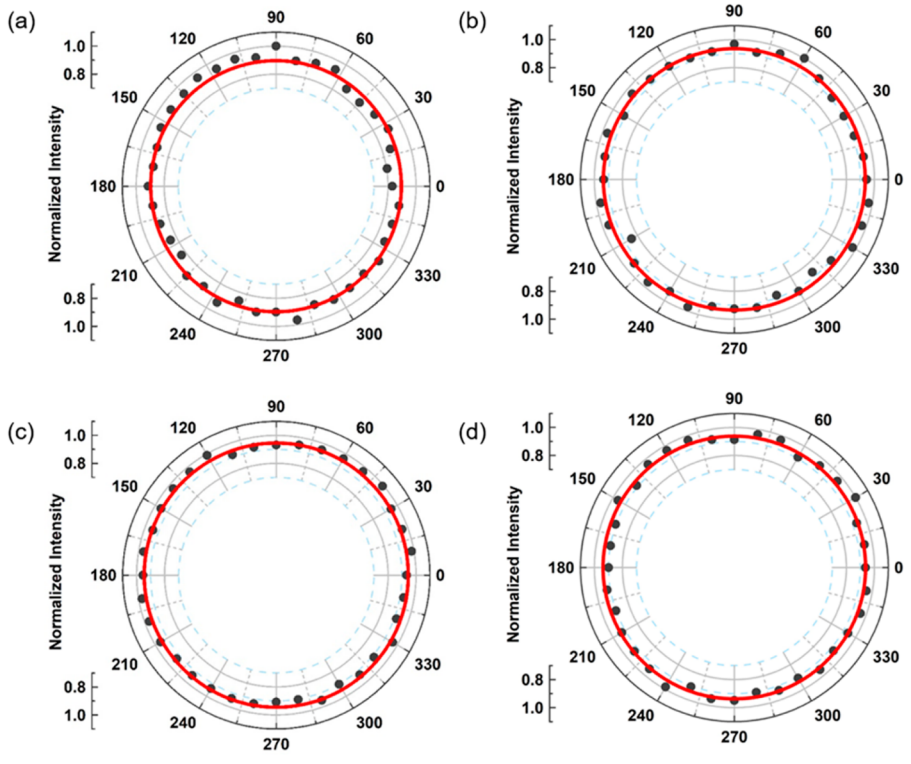

Figure 4. (a, b) Polar plots of UCL intensity as a function of the excitation laser polarization angle for the UCNPs on the glass and on the gold film, respectively. (c, d) Polar plots of the normalized UCL intensity at different polarization directions for the UCNPs on the glass and on the gold film, respectively.

the excitation laser at 980 nm and the nanoantenna array is too weak to produce the obvious polarization modification of the UCL.

Meanwhile, the emission polarization state of the UCL under different excitation polarizations was also investigated. The UCL intensity over the whole spectrum from 480 to 780 nm achieves

DOI: 10.1021/acs.jpcc.8b03975
J. Phys. Chem. C 2018, 122, 15666−15672

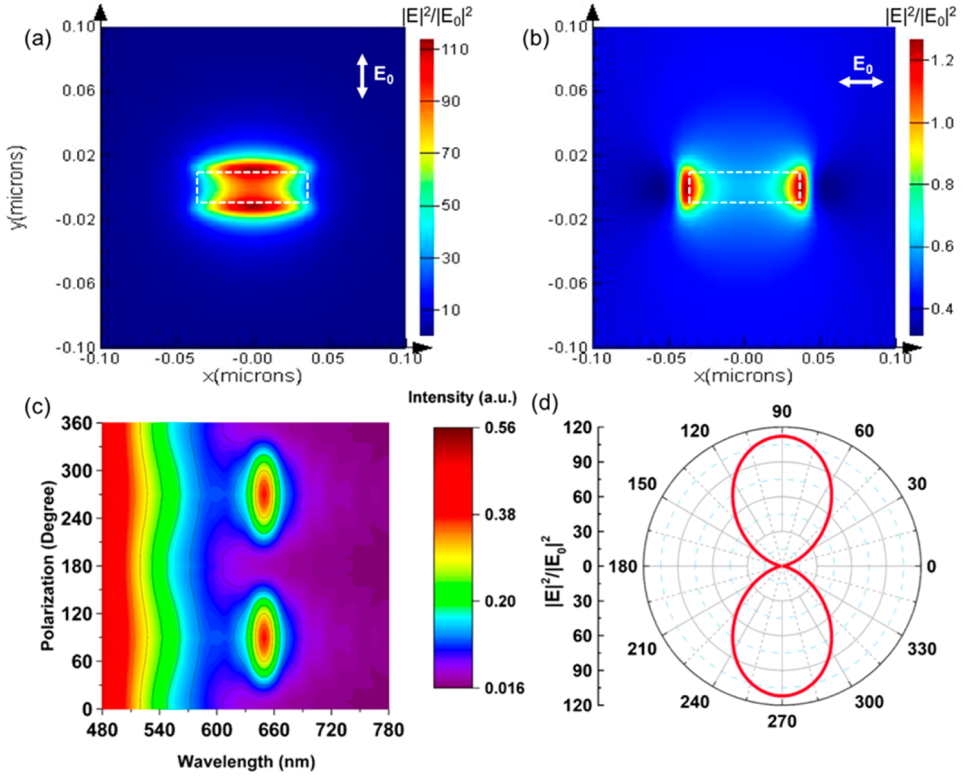

Figure 5. FDTD simulated electric field intensity enhancement images for (a) perpendicular and (b) parallel polarization at 660 nm, and the white dash line represents one rectangle slot. (c) Simulated absorption spectra of the plasmonic nanoantenna array as a function of incident polarization angle. (d) Polar plot of the simulated electric field enhancement at 660 nm dependent on the polarization angle.

maximum and minimum for polarization direction of excitation laser tuned along 90° and 0° respectively as depicted in Figure 2d. And the polarization state of the UCL was verified by rotating the half-wave plate before the Glan-Taylor prism in the detection part of the microscope system. To analyze the polarization state of the light, DOLP is used here

$$\mathrm{DOLP} = \frac{I_{\max} - I_{\min}}{I_{\max} + I_{\min}} \quad (2)$$

where I_{max} and I_{min} represent the maximal and the minimum UCL intensities, respectively. For a perfect linear polarization light, DOLP is 100%. Meanwhile, an unpolarized light has a DOLP of 0. The polarization state of the UCL at 550 and 660 nm was studied individually at the fixed excitation polarization angle of 90° and 0°, respectively. When the excitation polarization angle was 90°, as shown in Figure 3a, different UCL spectral components exhibit different polarization states when the localized surface plasmon resonance (LSPR) of the nanoantenna array selectively enhances the emission band of the whole UCL spectrum. The UCL peak at 660 nm shows strong linear polarization and the degree of polarization was calculated to be 80% as shown in Figure 3b. But that of the UCL peak at 550 nm was only 20%. Figure 3c shows the UCL spectra when excited by a horizontally polarized light (0°). The DOLP of the 660 nm UCL peak slightly declined to ~76%, and that of the UCL peak at 550 nm was still about 20% as shown in Figure 3d. It could be observed that both vertical and horizontal polarization excitation can lead to the similar UCL polarization state for the two UCL peaks. The little difference on the DOLP for the same UCL peak under different excitation polarization confirmed that nonplasmonic resonant excitation at 980 nm has little contribution on the polarization modification of the UCL.

More importantly, the polarization states for the UCL peaks at different wavelengths is quite different. The UCL peak at 660 nm is almost linearly polarized while the UCL peak at 550 nm is nearly unpolarized no matter whether the polarization direction of the excitation laser is perpendicular or parallel to the long axis of the nanoantenna slot. In other words, the polarization state of UCL peak at 660 nm was selectively tuned to be linear while that at 550 nm remained unpolarized. We actually measured the polarized UCL properties at 660 nm of several UCNPs in different positions on the slot nanoantenna array. The degrees of linear polarization varied from ~70% to 80%, which should be due to the location variation of UCNPs on the slot nanoantenna array. However, it is difficult to in situ measure polarized UCL of UCNP directly after locating the position of UCNP on the slot array by AFM.

For comparison, we also investigated the UCL polarization properties of single UCNP on the 50 nm thick gold film and on a clean cover glass. Because of the fact that the $NaYF_4$ nanocrystal is uniformly doped by Yb^{3+} and Er^{3+}, which shape is a symmetric sphere, as well as the fact that gold film and glass are isotropic interfaces, the UCL hardly shows any polarization property, as shown in Figure 4. In the UCL polarization spectrum, the DOLPs of UCL was 0% for both the UCNPs on the 50 nm thick gold film and that on the cover glass. We can conclude that the linear polarization of the UCL peak at 660 nm was induced by LSPR effect on the slot nanoantenna array.

To better understand the LSPR effect on UCL selective polarization tuning, we performed a simulation by FDTD method using the size of the rectangular slot. First, the LSPR near-field images at 660 nm were simulated in orthogonal polarizations of 90° and 0° as shown in Figure 5, parts a and b. The enhancement factor is proportional to the local near-field

DOI: 10.1021/acs.jpcc.8b03975
J. Phys. Chem. C 2018, 122, 15666−15672

enhancement $|E|^2/|E_0|^2$.When excited at 90°, the coupling by the surface plasmon polaritons from both lengths of the slot forms a "hot spot" with enhancement factor up to 110. However, when excited at 0°, the enhanced electric field locates at two ends of the rectangular slot and the overall intensity is less enhanced. The simulation implies that the gap distance along the excitation polarization direction is essential for the LSPR. Smaller gap will result in higher enhancement. Due to the unbalanced enhancements on the two orthogonal polarization directions, the polarization state of UCL was modified by the LSPR to be at 90°.

We also simulated the polarization LSPR spectrum as shown in Figure 5c. The simulated results agree with the experimental results of the extinction spectra in Figure 1b. Moreover, the spectral peak appeared near 650 nm shows quite strong polarization dependence. The maximum intensity appears at 90°, 270° while the minimum appears at 0°, 180°, 360°, which agrees with the experiment results. Meanwhile, the spectrum at 550 nm shows much less polarization dependence. The polar plot for the polarization at 660 nm in Figure 5d explains that as the LSPR wavelength matches the UCL wavelength at 660 nm the selective polarization modification of optical field of UCL can be achieved. The near-field enhancement at 550 nm dependent on the polarization angle was also simulated as shown in Figure S5. Comparing with the strong polarization sensitivity of the near-field enhancement at 660 nm in Figure 5d, that at 550 nm is less sensitive, and thus the UCL at 550 nm is nearly unpolarized for all polarization. Simulation at the excitation of 980 nm was also performed in Figure S6, showing less polarization dependence due to the weak plasmonic response of the nanoantenna array at 980 nm, which explains the experiment results about the weak excitation polarization dependence.

In the future, it may be interesting to design the width and length of the slots such that the long-wavelength extinction peak of the slot nanoantenna array can match with the 980 nm excitation wavelength and the short-wavelength extinction peak with either the red or green UCL band of UCNPs. Previous theoretical and experimental studies have demonstrated that the UCL intensity of UCNPs could be significantly increased by simultaneously enhancing the excitation and emission processes of UCNPs using such plasmonic dual-resonance nanostructures.[41,42] It can be expected that the polarization sensitivity of UCNPs on the slot nanoantenna array will be increased. The plasmon-induced selective polarization modification of the UCL of UCNPs on the slot nanoantenna array may find many applications. For example, for the application in polarization-based 3D display, comparing with polarized emission of quantum dots in plasmonic cavities and gallium nitride on the photonic crystals,[13,39] UCNPs with color-tunable emissions and high photothermal stability on the slot nanoantenna array may have an advantage over them. By comparing with unpolarized UCL in UCNP-labeled biological tissues, the imaging resolution and contrast will be improved when they are transferred to the plasmonic slot nanoantenna array, and thus it may promise potential applications in biodetection and imaging.

CONCLUSIONS

In summary, we demonstrate that the polarization of the UCL of β-$NaYF_4$:Yb^{3+},Er^{3+} nanoparticles can be selectively modified by using plasmonic rectangular slot nanoantenna array. The red emission band at 660 nm from spherical β-$NaYF_4$:Yb^{3+},Er^{3+} nanoparticles deposited on the nanoantenna array was modified to be almost linearly polarized, which was attributed to the resonant interaction between the red emission band at 660 nm of the UCNPs and the plasmonic modes of the rectangular slot nanoantenna array. For the UCL of the UCNP at 550 nm, only weak emission polarization was found due to its negligible interaction with the slot nanoantenna array. Meanwhile, the polarization direction of the excitation laser at 980 nm had little effect on the UCL polarization modification due to the weak response of the nanoantenna array to the excitation laser. All the experiment results could be well explained by the theoretical simulations based on the LSPR with the FDTD method. With further optimization of the gold nanoantenna array design and fabrication, this plasmon-induced selective polarization modification of the UCL is promising in that it yields a straightforward method to manipulate the polarization state for the applications in multicolor light source, polarization-based 3D display and biodetection and imaging.

ASSOCIATED CONTENT

Supporting Information

The Supporting Information is available free of charge on the ACS Publications website at DOI: 10.1021/acs.jpcc.8b03975.

TEM image and XRD pattern of UCNPs, AFM image of UCNPs on the nanoantenna array, scheme of experimental setup, confocal fluorescence image of a single UCNP on the nanoantenna array, FDTD simulation of near field enhancement at 550 and 980 nm, and absorption spectra from 800 to 1100 nm of the nanoantenna array (PDF)

AUTHOR INFORMATION

Corresponding Authors

*E-mail: btwu@phy.ecnu.edu.cn (B.W.).
*E-mail: ewu@phy.ecnu.edu.cn (E.W.).

ORCID

Botao Wu: 0000-0002-2598-3926

Notes

The authors declare no competing financial interest.

ACKNOWLEDGMENTS

This work was funded in part by the National Natural Science Fund of China (11722431, 11674099, 11621404, 61775106, 11711530205, and 91750204), the Natural Science Foundation of Shanghai (16ZR1409400), the Shuguang Program (15SG22), the Shanghai International Cooperation Project (16520710600), the National Special Funds for the Development of Major Scientific Research Instruments and Equipment (61227902), and the 111 Project (B12024, B07013) National Key R&D Program of China (2017YFA0305100, 2017YFA0303800); PCSIRT (IRT13R29).

REFERENCES

(1) Chatterjee, D. K.; Gnanasammandhan, M. K.; Zhang, Y. Small upconverting fluorescent nanoparticles for biomedical applications. *Small* **2010**, *6*, 2781−2795.

(2) Gai, S.; Li, C.; Yang, P.; Lin, J. Recent progress in rare earth micro/nanocrystals: soft chemical synthesis, luminescent properties, and biomedical applications. *Chem. Rev.* **2014**, *114*, 2343−2389.

(3) Dong, H.; Du, S. R.; Zheng, X. Y.; Lyu, G. M.; Sun, L. D.; Li, L. D.; Zhang, Z.; Zhang, C.; Yan, C. H. Lanthanide nanoparticles: from design toward bioimaging and therapy. *Chem. Rev.* **2015**, *115*, 10725−10815.

(4) Liu, Y.; Lu, Y.; Yang, X.; Zheng, X.; Wen, S.; Wang, F.; Vidal, X.; Zhao, J.; Liu, D.; Zhou, Z.; et al. Amplified stimulated emission in

DOI: 10.1021/acs.jpcc.8b03975
J. Phys. Chem. C 2018, 122, 15666−15672

upconversion nanoparticles for super-resolution nanoscopy. *Nature* **2017**, *543*, 229−233.
(5) Idris, N. M.; Gnanasammandhan, M. K.; Zhang, J.; Ho, P. C.; Mahendran, R.; Zhang, Y. In vivo photodynamic therapy using upconversion nanoparticles as remote-controlled nanotransducers. *Nat. Med.* **2012**, *18*, 1580−1585.
(6) Chen, G.; Qiu, H.; Prasad, P. N.; Chen, X. Upconversion nanoparticles: design, nanochemistry, and applications in theranostics. *Chem. Rev.* **2014**, *114*, 5161−5264.
(7) Downing, E.; Hesselink, L.; Ralston, J.; Macfarlane, R. A three-color, solid-state, three-dimensional display. *Science* **1996**, *273*, 1185−1189.
(8) Huang, X.; Han, S.; Huang, W.; Liu, X. Enhancing solar cell efficiency: the search for luminescent materials as spectral converters. *Chem. Soc. Rev.* **2013**, *42*, 173−201.
(9) van der Ende, B. M.; Aarts, L.; Meijerink, A. Lanthanide ions as spectral converters for solar cells. *Phys. Chem. Chem. Phys.* **2009**, *11*, 11081−11095.
(10) Wang, F.; Liu, X. G. Recent advances in the chemistry of lanthanide-doped upconversion nanocrystals. *Chem. Soc. Rev.* **2009**, *38*, 976−989.
(11) Zhou, J.; Liu, Q.; Feng, W.; Sun, Y.; Li, F. Upconversion luminescent materials: advances and applications. *Chem. Rev.* **2015**, *115*, 395−465.
(12) Zhou, J.; Chen, G.; Wu, E.; Bi, G.; Wu, B.; Teng, Y.; Zhou, S.; Qiu, J. Ultrasensitive polarized up-conversion of Tm^{3+}-Yb^{3+} doped β-$NaYF_4$ single nanorod. *Nano Lett.* **2013**, *13*, 2241−2246.
(13) Cadusch, J. J.; Panchenko, E.; Kirkwood, N.; James, T. D.; Gibson, B. C.; Webb, K. J.; Mulvaney, P.; Roberts, A. Emission enhancement and polarization of semiconductor quantum dots with nanoimprinted plasmonic cavities: towards scalable fabrication of plasmon-exciton displays. *Nanoscale* **2015**, *7*, 13816−13821.
(14) Green, K. K.; Wirth, J.; Lim, S. F. Nanoplasmonic upconverting nanoparticles as orientation sensors for single particle microscopy. *Sci. Rep.* **2017**, *7*, 762.
(15) Shi, S.; Sun, L.; Xue, Y.; Dong, H.; Wu, K.; Guo, S.; Wu, B.; Yan, C. Scalable direct writing of lanthanide-doped $KMnF_3$ perovskite nanowires into aligned arrays with polarized up-conversion emission. *Nano Lett.* **2018**, *18*, 2964−2969.
(16) Lu, K.; Zhao, Y. H. Experimental evidences of lattice distortion in nanocrystalline materials. *Nanostruct. Mater.* **1999**, *12*, 559−562.
(17) Ueno, K.; Juodkazis, S.; Shibuya, T.; Yokota, Y.; Mizeikis, V.; Sasaki, K.; Misawa, H. Nanoparticle plasmon-assisted two-photon polymerization induced by incoherent excitation source. *J. Am. Chem. Soc.* **2008**, *130*, 6928−6929.
(18) Wu, B.; Ueno, K.; Yokota, Y.; Sun, K.; Zeng, H.; Misawa, H. Enhancement of a two-photon-induced reaction in solution using light-harvesting gold nanodimer structures. *J. Phys. Chem. Lett.* **2012**, *3*, 1443−1447.
(19) Song, M.; Wu, B.; Chen, G.; Liu, Y.; Ci, X.; Wu, E.; Zeng, H. Photoluminescence plasmonic enhancement of single quantum dots coupled to gold microplates. *J. Phys. Chem. C* **2014**, *118*, 8514−8520.
(20) Ayala-Orozco, C.; Liu, J. G.; Knight, M. W.; Wang, Y.; Day, J. K.; Nordlander, P.; Halas, N. J. Fluorescence enhancement of molecules inside a gold nanomatryoshka. *Nano Lett.* **2014**, *14*, 2926−2933.
(21) Ming, T.; Zhao, L.; Chen, H.; Woo, K. C.; Wang, J.; Lin, H. Experimental evidence of plasmophores: plasmon-directed polarized emission from gold nanorod−fluorophore hybrid nanostructures. *Nano Lett.* **2011**, *11*, 2296−2303.
(22) Ming, T.; Zhao, L.; Yang, Z.; Chen, H.; Sun, L.; Wang, J.; Yan, C. Strong polarization dependence of plasmon-enhanced fluorescence on single gold nanorods. *Nano Lett.* **2009**, *9*, 3896−3903.
(23) Sugimoto, H.; Chen, T.; Wang, R.; Fujii, M.; Reinhard, B. M.; Dal Negro, L. Plasmon-enhanced emission rate of silicon nanocrystals in gold nanorod composites. *ACS Photonics* **2015**, *2*, 1298−1305.
(24) Fu, B.; Flynn, J. D.; Isaacoff, B. P.; Rowland, D. J.; Biteen, J. S. Super-resolving the distance-dependent plasmon-enhanced fluorescence of single dye and fluorescent protein molecules. *J. Phys. Chem. C* **2015**, *119*, 19350−19358.
(25) Yao, Y.; Yang, Z.; Hwang, J.; Su, H.; Haung, J.; Lin, T.; Shen, J.; Lee, M.; Tsai, M.; Lee, Y. Coherent and polarized random laser emissions from colloidal CdSe/ZnS quantum dots plasmonically coupled to ellipsoidal Ag nanoparticles. *Adv. Opt. Mater.* **2017**, *5*, 1600746.
(26) Fu, M.; Qian, L.; Long, H.; Wang, K.; Lu, P.; Rakovich, Y. P.; Hetsch, F.; Susha, A. S.; Rogach, A. L. Tunable plasmon modes in single silver nanowire optical antennas characterized by far-field microscope polarization spectroscopy. *Nanoscale* **2014**, *6*, 9192−9197.
(27) Andersen, S. K. H.; Kumar, S.; Bozhevolnyi, S. I. Ultrabright linearly polarized photon generation from a nitrogen vacancy center in a nanocube dimer antenna. *Nano Lett.* **2017**, *17*, 3889−3895.
(28) Cohen-Hoshen, E.; Bryant, G. W.; Pinkas, I.; Sperling, J.; Bar-Joseph, I. Exciton−plasmon interactions in quantum dot−gold nanoparticle structures. *Nano Lett.* **2012**, *12*, 4260−4264.
(29) Zhang, T.; Gao, N.; Li, S.; Lang, M.; Xu, Q. Single-particle spectroscopic study on fluorescence enhancement by plasmon coupled gold nanorod dimers assembled on DNA origami. *J. Phys. Chem. Lett.* **2015**, *6*, 2043−2049.
(30) Lu, G.; Li, W.; Zhang, T.; Yue, S.; Liu, J.; Hou, L.; Li, Z.; Gong, Q. Plasmonic-enhanced molecular fluorescence within isolated bowtie nano-apertures. *ACS Nano* **2012**, *6*, 1438−1448.
(31) Mertens, H.; Biteen, J. S.; Atwater, H. A.; Polman, A. Polarization-selective plasmon-enhanced silicon quantum-dot luminescence. *Nano Lett.* **2006**, *6*, 2622−2625.
(32) Ren, M.; Chen, M.; Wu, W.; Zhang, L.; Liu, J.; Pi, B.; Zhang, X.; Li, Q.; Fan, S.; Xu, J. Linearly polarized light emission from quantum dots with plasmonic nanoantenna arrays. *Nano Lett.* **2015**, *15*, 2951−2957.
(33) Zhu, Q.; Zheng, S.; Lin, S.; Liu, T.; Jin, C. Polarization-dependent enhanced photoluminescence and polarization-independent emission rate of quantum dots on gold elliptical nanodisc arrays. *Nanoscale* **2014**, *6*, 7237−7242.
(34) He, J. J.; Zheng, W.; Ligmajer, F.; Chan, C. F.; Bao, Z. Y.; Wong, K. L.; Chen, X. Y.; Hao, J. H.; Dai, J. Y.; Yu, S. F.; et al. Plasmonic enhancement and polarization dependence of nonlinear upconversion emissions from single gold nanorod@SiO_2@CaF_2: Yb^{3+}, Er^{3+} hybrid core−shell−satellite nanostructures. *Light: Sci. Appl.* **2016**, *6*, e16217.
(35) Xue, Y.; Ding, C.; Rong, Y.; Ma, Q.; Pan, C.; Wu, E.; Wu, B.; Zeng, H. Tuning plasmonic enhancement of single nanocrystal upconversion luminescence by varying gold nanorod diameter. *Small* **2017**, *13*, 1701155.
(36) Yun, H.; Lee, S. Y.; Hong, K.; Yeom, J.; Lee, B. Plasmonic cavity-apertures as dynamic pixels for the simultaneous control of colour and intensity. *Nat. Commun.* **2015**, *6*, 7133.
(37) Vrabioiu, A. M.; Mitchison, T. J. Structural insights into yeast septin organization from polarized fluorescence microscopy. *Nature* **2006**, *443*, 466−469.
(38) Chen, Z.; Li, H.; Jia, W.; Liu, X.; Li, Z.; Wen, F.; Zheng, N.; Jiang, J.; Xu, D. Bivalent aptasensor based on silver-enhanced fluorescence polarization for rapid detection of lactoferrin in milk. *Anal. Chem.* **2017**, *89*, 5900−5908.
(39) Matioli, E.; Brinkley, S.; Kelchner, K. M.; Hu, Y.; Nakamura, S.; DenBaars, S.; Speck, J.; Weisbuch, C. High-brightness polarized light-emitting diodes. *Light: Sci. Appl.* **2012**, *1*, e22.
(40) Lide, D. R. *CRC Handbook of Chemistry and Physics*; CRC Press: Boca Raton, FL, 2009.
(41) Liu, X.; Lei, D. Y. Simultaneous excitation and emission enhancements in upconversion luminescence using plasmonic double-resonant gold nanorods. *Sci. Rep.* **2015**, *5*, 15235.
(42) Kang, F.; He, J.; Sun, T.; Bao, Z. Y.; Wang, F.; Lei, D. Y. Plasmonic dual-enhancement and precise color tuning of gold nanorod@SiO_2 coupled core−shell−shell upconversion nanocrystals. *Adv. Funct. Mater.* **2017**, *27*, 1701842.

DOI: 10.1021/acs.jpcc.8b03975
J. Phys. Chem. C 2018, 122, 15666−15672